RESEARCH ARTICLE

CANCER

Adrenergic nerves activate an angio-metabolic switch in prostate cancer

Ali H. Zahalka,[1,2] Anna Arnal-Estapé,[1,2]* Maria Maryanovich,[1,2] Fumio Nakahara,[1,2] Cristian D. Cruz,[1,2] Lydia W. S. Finley,[3] Paul S. Frenette[1,2,4]†

Nerves closely associate with blood vessels and help to pattern the vasculature during development. Recent work suggests that newly formed nerve fibers may regulate the tumor microenvironment, but their exact functions are unclear. Studying mouse models of prostate cancer, we show that endothelial β-adrenergic receptor signaling via adrenergic nerve–derived noradrenaline in the prostate stroma is critical for activation of an angiogenic switch that fuels exponential tumor growth. Mechanistically, this occurs through alteration of endothelial cell metabolism. Endothelial cells typically rely on aerobic glycolysis for angiogenesis. We found that the loss of endothelial *Adrb2*, the gene encoding the β_2-adrenergic receptor, leads to inhibition of angiogenesis through enhancement of endothelial oxidative phosphorylation. Codeletion of *Adrb2* and *Cox10*, a gene encoding a cytochrome IV oxidase assembly factor, prevented the metabolic shift induced by *Adrb2* deletion and rescued prostate cancer progression. This cross-talk between nerves and endothelial metabolism could potentially be targeted as an anticancer therapy.

Solid tumors depend on angiogenesis to sustain their growth (*1*). The transition from hyperplasia to highly vascularized growing tumor, referred to as the "angiogenic switch," is a state in which proangiogenic factors—such as vascular endothelial growth factor (VEGF) and other secreted angiocrine factors—predominate over antiangiogenic signals (*2*). During development, peripheral nerves associate closely with growing blood vessels, organizing vascular pattern (*3*, *4*), a phenomenon that has also been described in models of wound healing (*5*, *6*). Emerging studies suggest that nerves can also regulate tumorigenesis (*7*–*11*). Sympathetic nerve fibers deliver adrenergic signals that act via β-adrenergic receptors (βAdRs) expressed in the tumor microenvironment. However, the cellular target(s) and molecular mechanism(s) responsible for neural regulation of cancer are not known and may provide novel therapeutic avenues.

Adrenergic nerves regulate angiogenesis in early tumor growth

To investigate the interplay between adrenergic nerves and early-stage tumor growth, we orthotopically implanted prostate cancer xenografts in immunodeficient Balb/c (*nu/nu*) mice. Xenografts exhibited exponential growth kinetics from ~18 days postimplantation (βAdR^{WT}) (Fig. 1A). By contrast, no substantial tumor growth occurred in *nu/nu* mice that were also genetically deficient in both β_2-adrenergic (*Adrb2*) and β_3-adrenergic (*Adrb3*) receptors (βAdR^{KO}) (*9*). Pathological examination of prostate tissues revealed that tumors formed in βAdR^{KO} recipients (Fig. 1A and fig. S1A) but their growth was arrested at day 18 (Fig. 1B), suggesting that βAdR signaling plays a key role in the molecular "switch" enabling exponential tumor growth. Before the switch, day-18 tumors from both control and βAdR^{KO} recipients showed no difference in size, vascular permeability, or hypoxic area (fig. S1, A to C). We next investigated the vascular density and tumor vasculature patterns by semi-automated analysis using Simple Neurite Tracer (*12*) in whole cross-sectional montages of day-18 tumors. These analyses revealed reductions in the density of tumor vessels (Fig. 1, C and D) due to significant alterations in the vascular patterns (reduced length and branching) in prostates of βAdR^{KO} mice compared with βAdR^{WT} controls (Fig. 1D). This observation suggests that the loss of adrenergic signaling in the tumor microenvironment may regulate angiogenesis.

To confirm these results in an independent assay, we orthotopically transplanted a cell-free type I collagen matrix into the prostate capsule of *nu/nu* mice, between the ventral prostate lobes. Because type I collagen is an angiogenic superpolymer (*13*) and mimics the changes in composition of the reactive extracellular matrix seen in prostate cancer (*14*, *15*), it promotes angiogenesis without the need to administer exogenous cytokines. We assessed recruitment of host vasculature into the matrix in control immunocompetent C57BL/6 mice and in mice chemically sympathectomized with 6-hydroxydopamine (6OHDA) (*9*). Analyses of vascular patterning revealed significant reductions in vessel migration, density, and branching in the denervated prostate matrices, as compared with controls (Fig. 1E). These data indicate that the vasculature serves as a stromal target for adrenergic nerves and that adrenergic signals modulate angiogenesis (*7*).

Endothelial ADRB2 controls the angiogenic switch

The angiogenic switch described above characterizes the progression of prostate cancer from the low-grade preneoplastic stage [low-grade prostatic intraepithelial neoplasia (LPIN)] (fig. S2, B and C) to the high-grade malignant stage [high-grade prostatic intraepithelial neoplasia (HPIN)] (Fig. 2A) (*16*). To explore the role of adrenergic signals in mediating angiogenesis in prostate cancer progression, we used the Hi-Myc (cMyc) spontaneous autochthonous prostate cancer mouse model. In these mice, the human *MYC* gene, driven by the probasin promoter, is overexpressed in the prostate; this leads to LPIN at 4 weeks, which progresses to HPIN by 8 weeks, followed by adenocarcinoma and finally invasive cancer by 24 weeks (*9*, *17*). This model recapitulates the histological changes seen in human disease (*18*, *19*). Immunofluorescence analyses of adrenergic nerves (tyrosine hydroxylase$^+$) and vessels ($CD31^+$) showed an increase in both nerve and vessel densities in the HPIN stage (Fig. 2A, and fig. S2A) but not in the preangiogenic LPIN stage (fig. S2, B and C). In addition, PIN progression coincided with an increased physical association of nerves and blood vessels (reduced proximity score; Fig. 2A). The levels of the β-adrenergic neurotransmitter noradrenaline were significantly elevated in HPIN prostates, whereas the levels of other catecholamines were unchanged (Fig. 2B). Analyses of *Adrb2* expression in prostate stromal populations implicated in tumor angiogenesis (*20*) revealed that *Adrb2* expression levels were highest in endothelial cells (fig. S3A).

To assess the specific contributions of *Adrb2* in stromal cells to cancer progression in the cMyc model, we conditionally deleted *Adrb2* by intercrossing $Adrb2^{fl/fl}$ (*21*) with Cre-expressing lines to delete the gene in myeloid cells [$Csf1r^{iCre}$ (*22*)], pericytes [$NG2^{CreERTM}$ (*23*)], or endothelial cells [$Cdh5\text{-}Cre^{ERT2}$ (*24*)]. Deletion of *Adrb2* in the targeted cells occurred at high efficiency (fig. S3, B to D). Deletion of *Adrb2* in pericytes during the LPIN stage did not result in a significant difference in prostate cancer weight in the HPIN stage or at the late adenocarcinoma stage (12 months of age), and no phenotype was also observed when *Adrb2* was deleted in myeloid cells (fig. S3, C and D). By contrast, deletion of *Adrb2* in

[1]Ruth L. and David S. Gottesman Institute for Stem Cell and Regenerative Medicine Research, Albert Einstein College of Medicine, Bronx, NY 10461, USA. [2]Department of Cell Biology, Albert Einstein College of Medicine, Bronx, NY 10461, USA. [3]Cell Biology Program, Memorial Sloan Kettering Cancer Center, New York, NY 10065, USA. [4]Department of Medicine, Albert Einstein College of Medicine, Bronx, NY 10461, USA.
*Present address: Department of Pathology, Yale School of Medicine, New Haven, CT 06520, USA. †Corresponding author. Email: paul.frenette@einstein.yu.edu

endothelial cells during the LPIN stage reduced progression to the HPIN stage (Fig. 2, C and D), and the inhibition of disease progression was sustained for more than 12 months (Fig. 2C). Histological analysis of *cMyc Adrb2*$^{fl/fl}$ *Cdh5-Cre*^{ERT2} mice (endothelial cell conditional knockout mice, henceforth referred to as *cMyc; Adrb2*^{ecKO}) revealed a significant reduction in Ki-67^{+} proliferative prostate epithelial cells (fig. S4A), which we confirmed by fluorescence-activated cell sorting (FACS) analysis (fig. S4B). The proliferation of prostate epithelial cells was reduced to levels seen at the LPIN stage before the angiogenic switch (fig. S2D), but without a significant change in epithelial apoptosis (fig. S4C). Thus, endothelial cells are the major stromal target of adrenergic nerves in the tumor microenvironment.

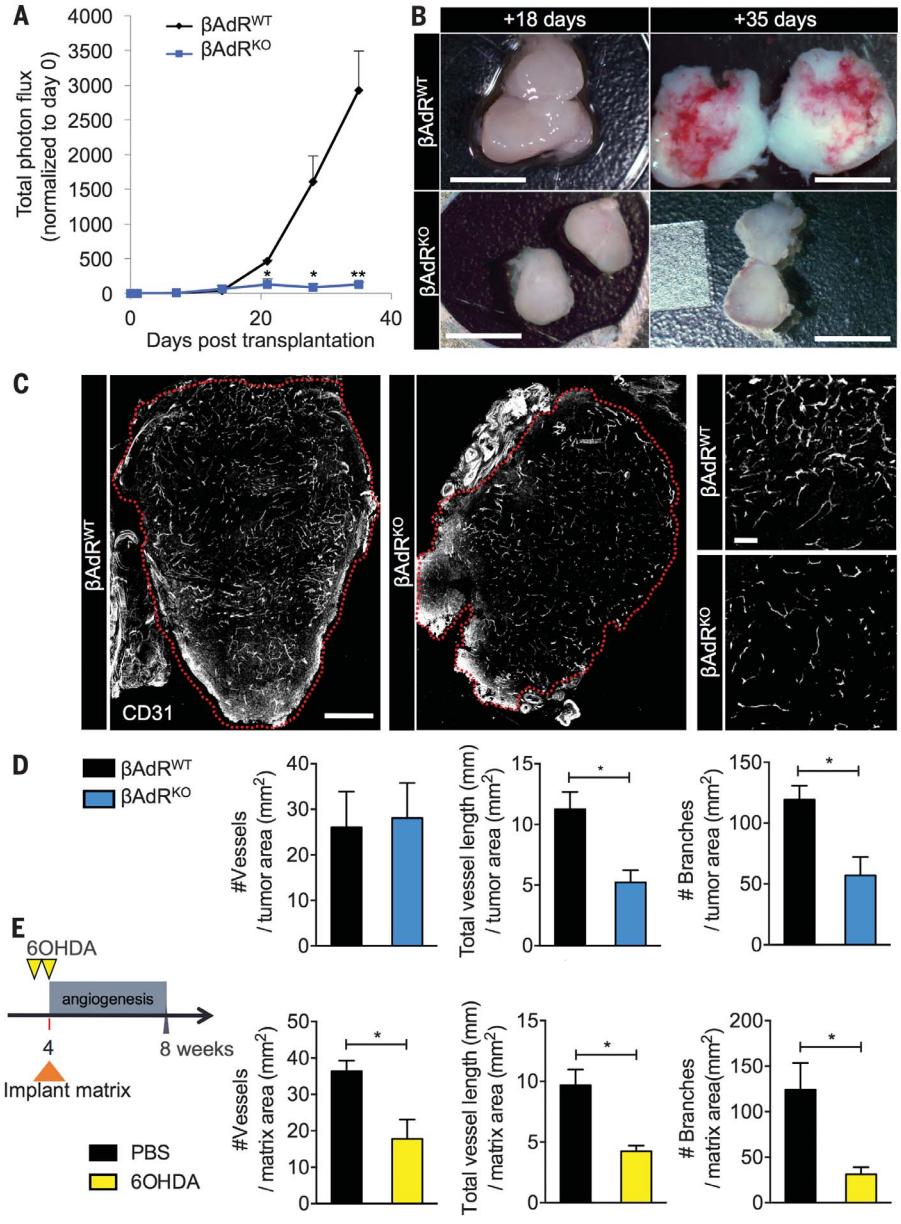

Fig. 1. Loss of β-adrenergic signaling in the prostate microenvironment arrests tumor growth and angiogenesis. (**A** to **D**) PC-3 cells stably expressing luciferase were orthotopically implanted into 8-week-old Balb/c *nu/nu* prostates. βAdR = Adrb2 + Adrb3. (A) Tumor growth was monitored in vivo weekly by bioluminescence. *n* = 6 mice per condition. (B) Comparison of orthotopic tumor size before (+18 days) and after (+35 days) angiogenic switch. Scale bars, 5 mm. (C) Immunofluorescence analyses of the vasculature in similar-sized tumors (outlined in red) before the angiogenic switch (+18 days). Cross-sectional montage of prostate xenografts from βAdR^{WT} (left) and βAdR^{KO} (middle) mice, and magnified view of βAdR^{WT} vasculature (right, top) and βAdR^{KO} vasculature (right, bottom). CD31 = vasculature. Montage scale bar, 500 μm; magnified-view scale bar, 100 μm. (D) Quantification of angiogenesis in orthotopic tumors (vessels traced using Simple Neurite Tracer). *n* = 4 mice per condition. (**E**) Experimental design and quantification of vessels recruited into orthotopic type I collagen matrix after sympathectomy with 6-hydroxydopamine (6OHDA). PBS = phosphate-buffered saline. *n* = 4 mice per condition. *P < 0.05; **P < 0.01. Error bars indicate SEM.

To evaluate the angiogenic switch during the transition from the LPIN to HPIN stage in prostate cancer progression (*16*), we induced endothelial *Adrb2* deletion in the cMyc model by administering tamoxifen to the mice at 4 weeks of age (LPIN stage). We then assessed angiogenesis and vascular patterning at 8 weeks (HPIN stage). Consistent with our results in the xenograft and denervation models (Fig. 1, D and E), we found that *cMyc; Adrb2*^{ecKO} mice exhibited a significant reduction in vessel density, migration, and branching 4 weeks after *Adrb2* gene deletion, as compared with *cMyc* controls (Fig. 2E and figs. S4D and S5, A and B). There was no significant change in pericyte coverage, vascular leakage, or tissue hypoxia (fig. S4, E to G). These data collectively suggest that adrenergic signals mediate an early angiogenic progression switch via endothelial *Adrb2*.

ADRB2 regulates oxidative metabolism in angiogenic prostate endothelial cells

To explore the molecular mechanisms underlying the angiogenic defect in *cMyc; Adrb2*^{ecKO} mice, we compared the transcriptome of endothelial cells isolated by FACS from *cMyc; Adrb2*^{ecKO} and *cMyc* prostates (Fig. 3A and fig. S6A). Gene set enrichment analysis revealed a highly significant increase in mitochondrial cytochrome c activity (fig. S6B). Among differentially expressed mitochondria-associated genes involved in metabolism, branched-chain keto acid dehydrogenase alpha peptide (*Bckdha*; involved in metabolizing branched-chain amino acids in the tricarboxylic acid cycle) and cytochrome c oxidase assembly factor 6 (*Coa6*; involved in the electron-transport chain) stood out by hierarchical cluster analysis (fig. S6C). Increased mRNA expression of both genes was validated by quantitative real-time polymerase chain reaction (fig. S6D). Consistent with our observation that *Adrb2* deletion in endothelial cells at the LPIN stage sustained inhibition of cancer progression 48 weeks after Cre-mediated recombination (Fig. 2C), we observed that *Coa6* expression remained elevated in *cMyc; Adrb2*^{ecKO} endothelial cells at that time point (fig. S6E). In addition, analysis of peritumoral and intratumoral endothelial cells isolated from the βAdR^{KO} orthotopic tumor model revealed increased expression of these mitochondrial genes (fig. S7, A and B). The effect of βAdR signals on genes involved in oxidative phosphorylation and vascular branching is reminiscent of recent studies showing that inhibition of glycolysis in endothelial cells alters angiogenesis during the development of retinal and hindbrain vessels (*25*, *26*).

To investigate the link between nerve-derived adrenergic signals and endothelial metabolism, we evaluated the change in endothelial mitochondrial membrane potential (Δψ), which

is associated with the accumulation of positively charged hydrogen ions in the mitochondrial intermembrane space during oxidative phosphorylation. We assessed $\Delta\psi$ in freshly isolated prostate endothelial cells by tetramethylrhodamine ethyl ester (TMRE) and quantified the quotient of basal-to-maximal nictotinamide adenine dinucleotide (reduced form, NADH) levels by autofluorescence, both measures of oxidative phosphorylation (*27*–*29*). We found that after progression to the HPIN stage, endothelial cell $\Delta\psi$ was reduced and the NADH quotient was increased without significant change in mitochondrial mass (fig. S8, A to D). Consistent with the notion that prostate endothelial cells operate at maximal respiratory capacity (RC), HPIN and wild-type (WT) prostate-derived endothelial cells did not exhibit spare RC, whereas significant spare RC was apparent in hematopoietic stem and progenitor cells isolated from the same animals (fig. S8E) (*29*). However, TMRE was significantly increased and NADH quotient reduced in freshly isolated endothelial cells from *cMyc; Adrb2*^{ecKO} mice (Fig. 3B and fig. S9A), consistent with enhanced oxidative phosphorylation. This was not due to a change in mitochondrial mass (fig. S9A) or to an effect on endothelial viability (fig. S9, B and C). In addition, we observed a similar increase in endothelial oxidative phosphorylation in orthotopic tumors in βAdR^{KO} recipients, as well as in WT mice subjected to adrenergic denervation (figs. S10, A and B, and S11, A and B). Endothelial glucose uptake was increased in the absence of *Adrb2* (Fig. 3C). These results strongly suggest that the loss of βAdR signaling enhances oxidative phosphorylation in endothelial cells.

To evaluate the role of βAdR in endothelial glucose metabolism, the main fuel source of endothelial cells (*25*, *30*), we knocked down *Adrb2* expression by lentiviral transduction of short hairpin RNA (shAdrb2) in primary mouse prostate endothelial cells that express the adenoviral *E4ORF1* gene; the latter gene allows the cells to survive in culture while maintaining their growth dependence on VEGF and fibroblast growth factor (*31*). shAdrb2 specifically inhibited *Adrb2* expression by 80% compared with control vector (shCntrl), without affecting endothelial cell viability or proliferation (fig. S12, A and B). In the presence of physiological levels of noradrenaline, shAdrb2 endothelial cells exhibited a marked increase in oxidative aerobic metabolism compared with shCntrl endothelial cells, as demonstrated by an increase in oxygen consumption (Fig. 3D). Like freshly isolated endothelial cells from *cMyc; Adrb2*^{ecKO} or βAdR^{KO} mice, endothelial cells treated with shAdrb2 showed an elevation in oxidative phosphorylation activity (increased $\Delta\psi$ and decreased NADH quotient), as well as an increase in glucose uptake, but no change in mitochondrial mass (fig. S13, A to C). Thus, this endothelial culture system recapitulates the metabolic profile of native prostate endothelial cells.

To explore the shift in endothelial metabolism that accompanies the loss of ADRB2 signaling, we assessed glucose uptake and the contributions of glucose-derived carbons to the tricarboxylic acid (TCA) cycle, an integral process that fuels oxidative phosphorylation. We observed increased glucose uptake in *cMyc; Adrb2*^{ecKO}-isolated endothelial cells compared with controls (Fig. 3C). We then traced the fate of uniformly labeled [U-^{13}C]-glucose in shCntrl and shAdrb2 endothelial cells cultured in the presence of noradrenaline. These experiments revealed a 1.9-fold increase in citrate levels in shAdrb2 compared with shCntrl endothelial cells (Fig. 3E), whereas lactate levels were unchanged (fig. S13D). Furthermore, shAdrb2 cells incorporated considerably more glucose-derived carbons into citrate than shCntrl cells (Fig. 3, F and G). Examination of isotopologue distribution

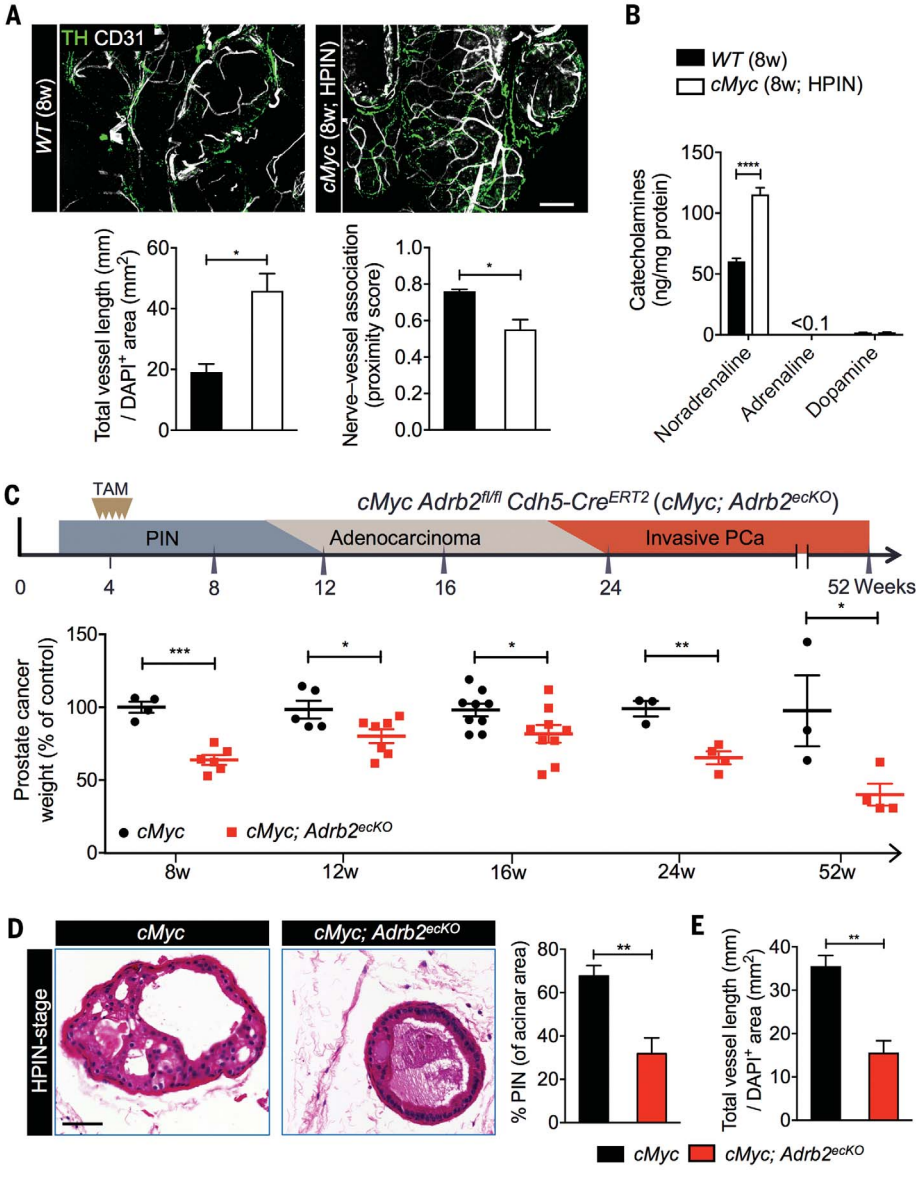

Fig. 2. Prostate endothelial cells closely associate with adrenergic nerves and require *Adrb2* for cancer progression and angiogenesis. (**A**) Thick-section images and quantification of the association between adrenergic nerves and the prostate vasculature in the high-grade prostatic intraepithelial neoplasia (HPIN) stage. Representative images of wild-type (WT) prostate (left, top) and HPIN-stage prostate (right, top). TH = tyrosine hydroxylase; CD31 = vasculature. Scale bar, 100 μm. Quantification of vessel density (left, bottom) and proximity of association between nerves and vessels (right, bottom). *n* = 4 mice per condition. DAPI = 4′,6-diamidino-2-phenylindole. (**B**) Catecholamine levels in HPIN-stage prostate quantified by high-performance liquid chromatography. *n* = 4 mice per condition. (**C**) *Cdh5-Cre*^{ERT2} deletion of *Adrb2* in endothelial cells and its effect at various histopathological stages (schema: top; prostate weight: bottom). TAM = tamoxifen; PCa = prostate cancer. (**D** and **E**) Effect of endothelial *Adrb2* deletion on HPIN pathology, as shown by (D) representative hematoxylin-and-eosin histology (left). Scale bar, 50 μm. Prevalence of PIN (right). *n* = 4 mice per condition. (E) Quantification of vascular density. *n* = 4 mice per condition. **P* < 0.05; ***P* < 0.01; ****P* < 0.001; *****P* < 0.0001. Error bars indicate SEM.

of glucose-derived citrate revealed an enrichment of m+2 isotopologue in shAdrb2 compared with shCntrl cells, reflective of pyruvate dehydrogenase–driven contribution of glucose-derived carbons into the TCA cycle (Fig. 3H). However, shAdrb2 endothelial cells were relatively depleted in the m+3 isotopologue, which may reflect a reduction in anaplerotic flux through pyruvate carboxylase (fig. S14A).

Because glutamine has been reported to be a major anaplerotic substrate in proliferating cells (*32*), we performed glutamine tracing experiments using uniformly labeled [U-^{13}C]-glutamine. We observed significant elevations in glutamine oxidation, as represented by an increase in labeled citrate levels and in the m+4 isotopologue in TCA cycle intermediates (fig. S14, B to D, and table S1). Consistent with the notion that accumulation of citrate may provide acetyl–coenzyme A for fatty acid synthesis (*33*), we also observed higher abundance of fatty acyl carnitines in shAdrb2 compared with control endothelial cells (fig. S14E). Furthermore, we found that adenosine triphosphate (ATP) levels were significantly elevated in shAdrb2 endothelial cells (Fig. 3I).

To dissect the relative contributions of glycolysis versus oxidative phosphorylation to ATP generation, we replaced glucose in the media with galactose (which forces cells to rely on oxidative phosphorylation for ATP production). This led to a substantial reduction in ATP levels in shCntrl cells, whereas no change in ATP levels was observed in shAdrb2 cells (fig. S15A). Inhibition of oxidative phosphorylation with antimycin A also reduced ATP levels to those seen in control cells (Fig. 3I), further indicating that depletion of ADRB2 shifts endothelial metabolism to oxidative phosphorylation. Taken together, the results obtained with multiple model systems and analytical methods show that the loss of βAdR signaling alters endothelial metabolism, enhancing oxidative phosphorylation.

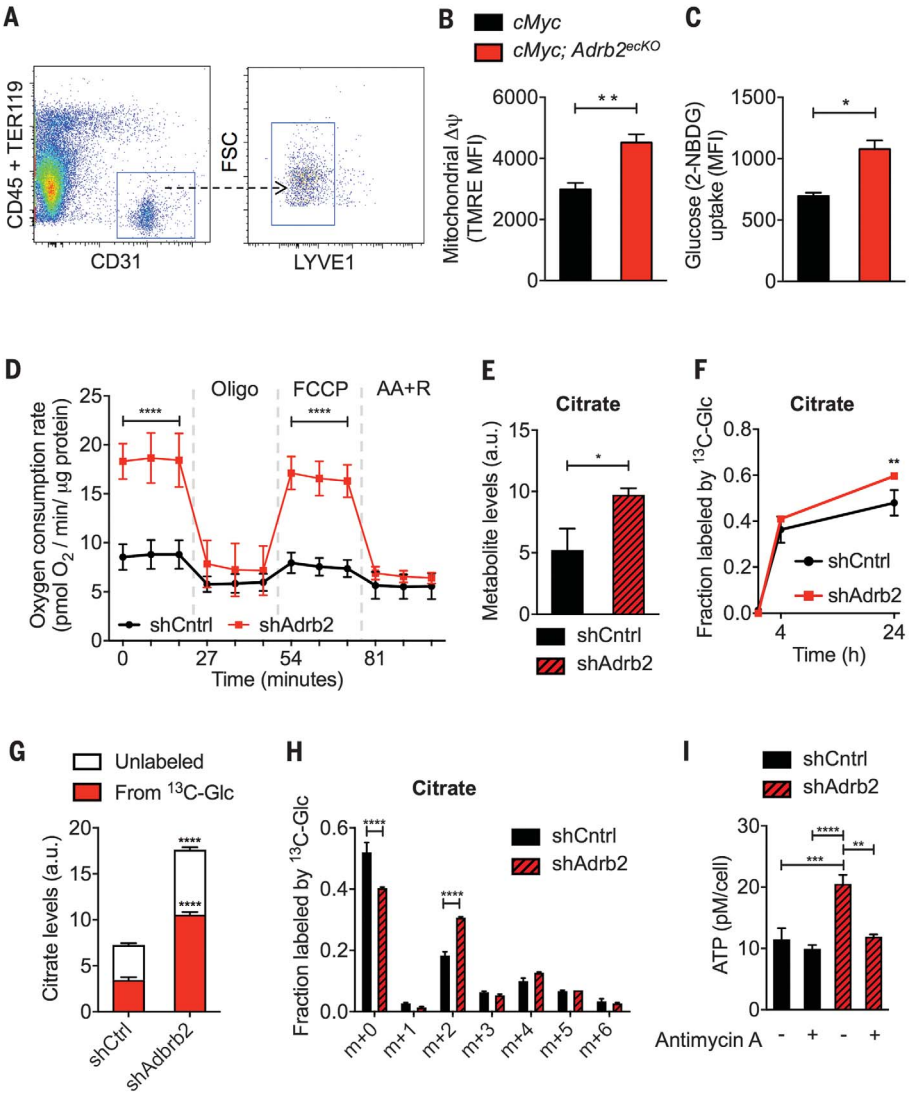

Fig. 3. *Adrb2* depletion increases endothelial oxidative metabolism. (**A** to **C**) FACS analysis of HPIN-stage endothelial cells. (A) Representative endothelial isolation plot from prostates. FSC = forward scatter. (B) Quantification of mitochondrial membrane potential (Δψ) by tetramethylrhodamine ethyl ester (TMRE) staining. *n* = 5 mice per condition. MFI = mean fluorescence intensity. (C) Quantification of endothelial glucose uptake by 2-NBDG. *n* = 6 or 7 mice per condition. (**D** to **I**) Metabolism and ATP production were assessed in shCntrl and shAdrb2 primary prostate endothelial cells after incubation with noradrenaline. (D) Oxygen consumption rates at baseline and in the presence of oligomycin, FCCP [carbonyl cyanide *p*-(trifluoromethoxy) phenylhydrazone], and antimycin A + rotenone (AA+R). *n* = 4 independent experiments. Error bars indicate SD. (E to H) Different analyses from the same set of experiments. *n* = 3 replicates per condition per time point. Metabolite levels were normalized to an internal standard and to sample protein content. (E) Intracellular levels of the tricarboxylic acid cycle metabolite citrate. a.u., arbitrary units. (F) Total fraction of citrate containing ^{13}C-label from [U-^{13}C]-glucose. (G) Relative intracellular levels of citrate labeling derived from [U-^{13}C]-glucose at 24 hours. (H) Fraction of each isotopologue of citrate (mass isotopologue distribution) after culture in 5 mM [U-^{13}C]-glucose for 24 hours. (I) Measurement of intracellular ATP levels in the presence or absence of antimycin A, an inhibitor of the electron transport chain. *n* = 3 independent experiments. **P* < 0.05; ***P* < 0.01; ****P* < 0.001; *****P* < 0.0001. Error bars indicate SEM.

Increased endothelial COA6 activity mediates the shift toward oxidative phosphorylation

To obtain further insight into the mechanism linking adrenergic signaling, altered metabolism, and endothelial cell function, we assessed the migration of *Adrb2*-sufficient (shCntrl) and *Adrb2*-deficient (shAdrb2) endothelial cells in an in vitro wound assay. We found that migration of shAdrb2 cells was markedly inhibited compared with that of shCntrl cells (fig. S16, A to C). Staining for α-tubulin revealed altered microtubule directional orientation in the shAdrb2 cells (fig. S16D). Endothelial cells require polarization of their microtubule cytoskeleton for directional migration (*34*), and microtubule organization regulates ATP-intensive actin cytoskeletal organization (*35*), which suggests that elevated ATP levels from oxidative metabolism may inhibit endothelial angiogenic function by altering cytoskeletal activity. In line with our transcriptome analysis (fig. S6, C and D), shAdrb2 increased *Coa6* mRNA and protein levels (fig. S15, B and C) but did not alter *Bckdha* expression, indicating that changes in *Coa6* expression may drive the observed metabolic alterations. Cyclic adenosine monophosphate, the second messenger generated by adenylyl cyclase (AC) upon βAdR signaling, was undetectable after noradrenaline stimulation in shAdrb2 cells but was present at high levels in control endothelial cells (fig. S15D). AC inhibition up-regulated *Coa6* expression in control cells, and conversely, AC stimulation with forskolin repressed *Coa6* in shAdrb2 endothelial cells (fig. S15E). These data indicate that ADRB2 signaling in endothelial cells regulates *Coa6* expression.

To assess whether these mitochondrial genes were sufficient to increase oxidative phosphorylation

and inhibit the angiogenic switch in prostate cancer, we overexpressed *Coa6* or *Bckdha* by lentiviral transduction in culture-expanded prostate endothelial cells. Whereas *Bckdha* did not induce a significant change in oxidative phosphorylation, *Coa6* overexpression (Coa6-GFP) (fig. S17A) substantially augmented endothelial oxidative metabolism (Fig. 4A and fig. S17B). In addition, Coa6–green fluorescent protein (GFP) significantly inhibited endothelial cell migration and proliferation but did not affect endothelial cell viability (fig. S17, C and D). To assess the effect of increased oxidative phosphorylation on angiogenesis in vivo, we orthotopically cotransplanted Coa6-GFP endothelial cells with human PC-3 prostate cancer cells into *nu/nu* males. In the prostate tumors, GFP^+ vessel quantification revealed a marked reduction in angiogenesis and tip cell formation in Coa6-GFP xenografts compared with xenografts produced by cotransplantation of PC-3 cells with Cntrl-GFP endothelial cells (Fig. 4, B and C). These results suggest that the loss of adrenergic signaling by *Adrb2* deletion increases *Coa6* expression, which causes an increase in oxidative phosphorylation, and that this metabolic shift inhibits angiogenesis.

To assemble cytochrome c oxidase (also known as complex IV), the terminal enzyme in oxidative phosphorylation that transfers electrons to molecular oxygen, COA6 cooperates with several factors, including the protein product of *Cox10* [heme A:farnesyltransferase cytochrome c oxidase assembly factor (*36*)]. Because conditional *Cox10* deletion has been shown to reduce oxidative phosphorylation in vivo in skeletal muscle (*37*), we interbred the $Cox10^{fl/fl}$ and *cMyc; Adrb2*$^{fl/fl}$*; Cdh5-Cre*^{ERT2} mouse strains (referred to as *cMyc; Adrb2*^{ecKO}*; Cox10*^{ecKO}). We found that conditional *Cox10* deletion in *cMyc; Adrb2*^{ecKO}*; Cox10*^{ecKO} prevented the metabolic switch to oxidative phosphorylation in endothelial cells induced by *Adrb2* deletion (Fig. 4D and fig. S18, A to C). Additionally, *Cox10* deletion rescued vascular perfusion of the prostate (fig. S19A), angiogenesis (Fig. 4E and fig. S19, B and C), and PIN cancer progression (Fig. 4F and figs. S18, D and E, and S20, A to C), without affecting endothelial proliferation or viability (fig. S20, D and E). Thus, the shift to endothelial oxidative metabolism is sufficient to inhibit the PIN-stage progression switch.

Discussion

Our results elucidate a critical link between neural signals in the tumor microenvironment and angiogenesis, wherein inhibition of adrenergic nerve activity alters endothelial metabolism to prevent the angiogenic switch that supports aggressive prostate cancer. The loss of βAdR signaling increases oxidative phosphorylation in endothelial cells via increased expression of the mitochondrial cytochrome c oxidase assembly factor COA6, inhibiting angiogenesis.

Endothelial cell metabolism represents an emerging targetable pathway for the treatment of vascular diseases (*38*). For example, activation of oxidative phosphorylation in renal endothelium protects against postischemic reperfusion injury in the kidneys (*39*), and inhibition of endothelial cell glycolysis prevents pathologic angiogenesis in ophthalmologic diseases (*40*). Our results suggest that endothelial cell metabolism can be locally regulated by nerves.

Nerves and vessels are tightly associated during development, sharing patterning cues (*41*). As tumors need to redevelop a vascular network to ensure nutrition and communication, neural input may provide a critical set of signals that coordinate cancer progression (*9*). Our results suggest that adrenergic signals promote the angiogenic switch in prostate cancer and that their inhibition (e.g., using β-blockers) could prevent or delay the dominance of proangiogenic factors that allow tumor progression.

Therapies attempting to starve the tumor by inhibiting angiogenesis have had limited long-term therapeutic benefit in various cancers, including that of the prostate (*42*), most likely due to resistance mechanisms (*43*). Cotargeting angiogenesis with neural signals and/or endothelial cell

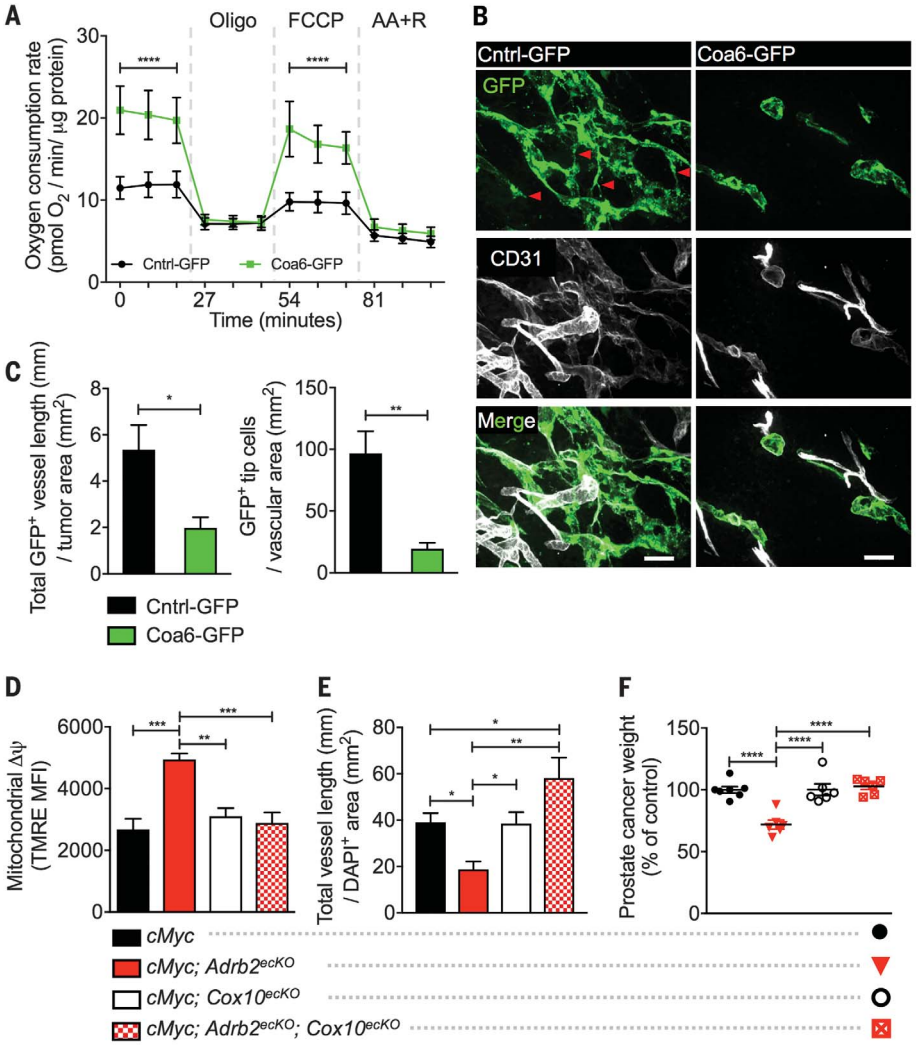

Fig. 4. Increased endothelial oxidative metabolism inhibits angiogenesis, and conditional *Cox10* deletion rescues endothelial metabolism, angiogenesis, and cancer progression. (**A**) Effect of *Coa6* overexpression (Coa6-GFP) on oxygen consumption rates at baseline and in the presence of oligomycin, FCCP, and antimycin A + rotenone (AA+R). $n = 4$ independent experiments. Error bars indicate SD. (**B** and **C**) Immunofluorescent analysis of orthotopically cotransplanted Cntrl-GFP or Coa6-GFP endothelial cells and PC-3 tumor cells to assess in vivo vessel formation. (B) Cntrl-GFP vessels, left; Coa6-GFP vessels, right. GFP = transplanted GFP-tagged endothelial cells; CD31 = vasculature. GFP^+ tip cells are indicated by red arrowheads. Scale bars, 50 µm. (C) Quantification of vessel density (left) and tip cell formation (right). $n = 3$ mice per condition. (**D** to **F**) HPIN-stage FACS analysis of $\Delta\psi$ (D), vessel density (E), and prostate cancer weight (F) in *cMyc*, *cMyc; Adrb2*^{ecKO}, *cMyc; Cox10*^{ecKO}, and double *cMyc; Adrb2*^{ecKO}*; Cox10*^{ecKO} mice, showing restoration of glycolitic metabolism, angiogenesis, and cancer progression after codeletion of *Adrb2* and *Cox10* in endothelial cells. $n = 6$ or 7 mice per condition. Error bars indicate SEM. *$P < 0.05$; **$P < 0.01$; ***$P < 0.001$; ****$P < 0.0001$.

metabolism may thus provide a multipronged therapeutic approach with the potential to overcome antiangiogenic resistance.

REFERENCES AND NOTES

1. J. Folkman, K. Watson, D. Ingber, D. Hanahan, *Nature* **339**, 58–61 (1989).
2. G. Bergers, L. E. Benjamin, *Nat. Rev. Cancer* **3**, 401–410 (2003).
3. Y. S. Mukouyama, D. Shin, S. Britsch, M. Taniguchi, D. J. Anderson, *Cell* **109**, 693–705 (2002).
4. W. Li *et al.*, *Dev. Cell* **24**, 359–371 (2013).
5. A. J. Ekstrand *et al.*, *Proc. Natl. Acad. Sci. U.S.A.* **100**, 6033–6038 (2003).
6. P. Martin, *Science* **276**, 75–81 (1997).
7. S. W. Cole, A. S. Nagaraja, S. K. Lutgendorf, P. A. Green, A. K. Sood, *Nat. Rev. Cancer* **15**, 563–572 (2015).
8. D. He *et al.*, *Hum. Pathol.* **52**, 182–189 (2016).
9. C. Magnon *et al.*, *Science* **341**, 1236361 (2013).
10. J. L. Saloman *et al.*, *Proc. Natl. Acad. Sci. U.S.A.* **113**, 3078–3083 (2016).
11. C. M. Zhao *et al.*, *Sci. Transl. Med.* **6**, 250ra115 (2014).
12. M. H. Longair, D. A. Baker, J. D. Armstrong, *Bioinformatics* **27**, 2453–2454 (2011).
13. T. Twardowski, A. Fertala, J. P. Orgel, J. D. San Antonio, *Curr. Pharm. Des.* **13**, 3608–3621 (2007).
14. J. A. Tuxhorn *et al.*, *Clin. Cancer Res.* **8**, 2912–2923 (2002).
15. N. Burns-Cox, N. C. Avery, J. C. Gingell, A. J. Bailey, *J. Urol.* **166**, 1698–1701 (2001).
16. W. J. Huss, C. F. Hanrahan, R. J. Barrios, J. W. Simons, N. M. Greenberg, *Cancer Res.* **61**, 2736–2743 (2001).
17. K. Ellwood-Yen *et al.*, *Cancer Cell* **4**, 223–238 (2003).
18. M. Ittmann *et al.*, *Cancer Res.* **73**, 2718–2736 (2013).
19. T. Iwata *et al.*, *PLOS ONE* **5**, e9427 (2010).
20. P. Carmeliet, R. K. Jain, *Nature* **473**, 298–307 (2011).
21. E. Hinoi *et al.*, *J. Cell Biol.* **183**, 1235–1242 (2008).
22. L. Deng *et al.*, *Am. J. Pathol.* **176**, 952–967 (2010).
23. X. Zhu *et al.*, *Development* **138**, 745–753 (2011).
24. I. Sörensen, R. H. Adams, A. Gossler, *Blood* **113**, 5680–5688 (2009).
25. K. De Bock *et al.*, *Cell* **154**, 651–663 (2013).
26. K. Wilhelm *et al.*, *Nature* **529**, 216–220 (2016).
27. Y. H. Wang *et al.*, *Cell* **158**, 1309–1323 (2014).
28. F. Kocabas, J. Zheng, C. Zhang, H. A. Sadek, *Methods Mol. Biol.* **1185**, 155–164 (2014).
29. M. Maryanovich *et al.*, *Nat. Commun.* **6**, 7901 (2015).
30. A. Krützfeldt, R. Spahr, S. Mertens, B. Siegmund, H. M. Piper, *J. Mol. Cell. Cardiol.* **22**, 1393–1404 (1990).
31. M. Seandel *et al.*, *Proc. Natl. Acad. Sci. U.S.A.* **105**, 19288–19293 (2008).
32. T. Cheng *et al.*, *Proc. Natl. Acad. Sci. U.S.A.* **108**, 8674–8679 (2011).
33. J. Munger *et al.*, *Nat. Biotechnol.* **26**, 1179–1186 (2008).
34. K. A. Hotchkiss *et al.*, *Mol. Cancer Ther.* **1**, 1191–1200 (2002).
35. R. Suzuki, K. Hotta, K. Oka, *Sci. Rep.* **5**, 16874 (2015).
36. A. Ghosh *et al.*, *Hum. Mol. Genet.* **23**, 3596–3606 (2014).
37. F. Diaz, C. K. Thomas, S. Garcia, D. Hernandez, C. T. Moraes, *Hum. Mol. Genet.* **14**, 2737–2748 (2005).
38. M. Potente, P. Carmeliet, *Annu. Rev. Physiol.* **79**, 43–66 (2017).
39. S. Liu, Y. Soong, S. V. Seshan, H. H. Szeto, *Am. J. Physiol. Renal Physiol.* **306**, F970–F980 (2014).
40. S. Schoors *et al.*, *Cell Metab.* **19**, 37–48 (2014).
41. A. Eichmann, I. Brunet, *Sci. Transl. Med.* **6**, 252ps9 (2014).
42. J. B. Aragon-Ching, R. A. Madan, W. L. Dahut, *J. Oncol.* **2010**, 361836 (2010).
43. G. Bergers, D. Hanahan, *Nat. Rev. Cancer* **8**, 592–603 (2008).

ACKNOWLEDGMENTS

We thank G. Karsenty, R. H. Adams, and J. W. Pollard for *Adrb2*$^{fl/fl}$, *Cdh5-Cre*^{ERT2}, and *Csf1r-iCre* mice, respectively, and M. Ginsberg (Angiocrine Bioscience) for primary mouse prostate endothelial cells. We also thank C. Prophete, P. Ciero, S. Pierce, J. F. Reidhaar-Olson, P. Guo, X. L. Du, M. Hanoun, L. Tesfa, Y. Qiu, and I. L. Kurland for advice and technical support; A. Beck for assistance with pathology; A. Zahalka for assistance programming in R; and L. Schwartz, S. K. Libutti, H. Pierce, S. Murillo, T. Mizoguchi, and S. Pinho for critical advice. We are grateful for grant support from the NIH (HL097700, DK056638, and HL069438 to P.S.F.) and the New York State Department of Health (C029154 and C030318GG to P.S.F.). A.H.Z. received the Junior Investigator Neuroscience Research Award from the Albert Einstein College of Medicine and was supported by grant F30CA203446 from the National Cancer Institute and NIH training grants T32 NS007098 and GM007288. M.M. is a New York Stem Cell Foundation Druckenmiller Fellow and was supported by the European Molecular Biology Organization (EMBO) European Commission FP7 (Marie Curie Actions, EMBOCOFUND2012, GA-2012-600394, ALTF 447-2014). F.N. was supported by a Postdoctoral Fellowship for Research Abroad from the Japan Society for the Promotion of Science. This work was also supported by NIH shared equipment grant 1S10OD019961 and NIH Diabetes and Research Training Center grant P60DK020541.

SUPPLEMENTARY MATERIALS

www.sciencemag.org/content/358/6361/321/suppl/DC1
Materials and Methods
Figs. S1 to S20
Table S1
References (*44*–*48*)

7 July 2016; resubmitted 25 July 2017
Accepted 1 September 2017
10.1126/science.aah5072

Adrenergic nerves activate an angio-metabolic switch in prostate cancer

Ali H. Zahalka, Anna Arnal-Estapé, Maria Maryanovich, Fumio Nakahara, Cristian D. Cruz, Lydia W. S. Finley and Paul S. Frenette

Science **358** (6361), 321-326.
DOI: 10.1126/science.aah5072

Tumor angiogenesis gets nervous

The microenvironment of solid tumors hosts many intercellular conversations that can either enhance or inhibit tumor growth. Interestingly, the tumor cells need not be direct participants in these conversations. Zahalka *et al.* studied genetically manipulated mouse models and found that adrenergic signals from autonomic nerves in the prostate cancer microenvironment fueled tumor growth by altering the metabolism of blood vessel endothelial cells (see the Perspective by Hayakawa and Wang). These nerve-derived signals suppressed oxidative phosphorylation in the endothelial cells, activating an angiogenic switch that facilitated rapid tumor growth. This cross-talk between nerves and endothelial cells could potentially offer a target for cancer therapies.

Science, this issue p. 321; see also p. 305